This is a peer-reviewed, accepted author manuscript of the following research article: Shankar, S, Chattopadhyaya, S, Mehta, KP & Vilaça, P 2024, 'A novel approach for zero material loss (zero flash) and uniform cross-section during friction stir welding of dissimilar thickness Cu and Al alloys', *Materials Chemistry and Physics*, vol. 326, 129859. https://doi.org/10.1016/j.matchemphys.2024.129859

A Novel Approach for Zero Material Loss (Zero Flash) and Uniform Cross-Section During Friction Stir Welding of Dissimilar Thickness Cu and Al Alloys

Sachindra Shankar[a], Somnath Chattopadhyaya[b], Kush P. Mehta[c], Pedro Vilaça[d]

[a]*Department of Mechanical Engineering, Anurag University, Hyderabad 500088, India*

[b]*Department of Mechanical Engineering, Indian Institute of Technology (Indian School of Mines), Dhanbad 826004, India*

[c]*Department of Design, Manufacturing and Engineering Management, University of Strathclyde, Glasgow, United Kingdom*

[d]*Department of Mechanical Engineering, School of Engineering, Aalto University, FI-02150 Espoo, Finland*

Abstract

A novel approach for getting a uniform weld cross-section and flash-free joint with the help of friction stir welding (FSW) is implemented. The influence of the tool tilt angle and rotational speed on the macrostructure, microstructure, and mechanical properties was investigated. Mechanical characterization techniques like an optical microscope, FESEM, profilometer, tensile test, bent test, and XRD analysis were used to evaluate the joint properties. A maximum tensile strength of 108.91 MPa was achieved, which led to a joint efficiency of 96.38 %. A maximum bending angle of 107˚ was achieved for samples S5 and S6. The Al/Cu mixed region in the stir zone displayed a maximum micro-hardness of 152.26 HV whereas a minimum micro-hardness of 33.57 HV was achieved in the HAZ along aluminium side. Welds prepared at a rotational speed of 540 RPM and a tool tilt angle of 4.5˚results in an almost flash-free joint.

Keywords: Friction Stir Welding, Aluminium Alloys, Copper alloys, Inclined bed, Tool Tilt Angle

1.Introduction

Combining copper (Cu) and aluminium (Al) can provide specific advantages in terms of mechanical and electrical qualities when used in joint or hybrid bus bar materials [1]. Conductivity, weight, cost, and corrosion resistance are a few of the characteristics that frequently affect the decision between copper and aluminium. Copper has higher electrical conductivity compared to aluminium. Therefore, copper is often preferred for applications where low electrical resistance is critical. Aluminium is significantly lighter than copper, which can be advantageous in applications where weight is a concern, such as transportation (e.g., hybrid bus bars).

Joining dissimilar thickness aluminum-copper (Al-Cu) alloys can be challenging due to the differences in material properties and thermal conductivity [2]. However, there are several methods that can be considered for joining dissimilar-thickness Al-Cu alloys [3]. Friction Stir Welding (FSW) is a solid-state welding process well-suited for joining dissimilar materials. The process involves using a rotating, non-consumable tool to generate frictional heat between the materials being joined[4–7]. This heat softens the materials without melting, allowing for a strong metallurgical bond.

In the context of FSW, "flash" typically refers to excess material displaced and protruding from the weld seam [8]. Various factors can influence flash formation, and addressing these issues is essential to ensure a high-quality weld. Here are some common factors and solutions related to flash formation in Friction Stir Welding. Dialami et al. observed that the major reason for flash formation is the excessive heat input caused by the increment in rotational speed [9]. Shankar et al. confirmed that the formation of a flash can be controlled by choosing an optimum tool tilt angle [10].

It has been observed in previous studies that the FSW is a suitable technique for joining dissimilar materials with different thicknesses [10–12]. However, Welding both materials becomes challenging if the copper is situated at the bottom or if there's a 3 mm difference in surface levels, primarily due to the significant gap between them. [13]. Straight penetration of the tool is restricted by the Al surface, which is on the upper side. At the same time, there is a big gap between the shoulder surface and the Cu plate, which restricts the proper plunging of material under the shoulder region. Thus, the joining between the materials is only due to the diffusion, which results in the unacceptable quality of the weld. Conversely, under the inclined

bed condition of 4.30 degrees, there is potential for weld formation despite some interfacial and root defects. The problem of root and interfacial defects can be solved by increasing the bed inclination up to such an extent that the participating material would be wholly locked under the shoulder region.

The current study aims to weld dissimilar thickness Al-Cu materials when the difference in top surface level between two materials is 3 mm. The method also compares the effect of different rotational speed and bed inclination angle combinations on the flash formation, weld cross-sectional uniformity, and weld quality. From the result, it has been observed that increasing the tilt angle reduces the flash formation on the weld surface. Also, with increasing tool tilt angle values, the axial plunge load increases, pushing the material downward and preventing it from spreading outside. In addition to that, the method also investigates the effect of a flat conical pin and zero tool offsets on the weld quality. The results revealed a sound and defect-free weld in almost every condition.

2. Experiments and Methodologies

The oxygen free copper (Cu min 99.99 %, O2 max 10 ppm) and aluminium alloy 1050 (0.25 wt.% Si, 0.40 wt.% Fe, 0.05 wt.% Cu, 0.05 wt.% Mg, 0.07 wt.% Zn and bal. Al) of 160 mm x 75 mm dimensions were used for the experiments. Thermo- mechanical properties of both the materials are incorporated in Table 2.1. A bed inclination angle of 8.65˚ was used to align the shoulder with the plates properly. The samples prepared at different parameters are shown in Table 2.2, whereas the fixed parameters are shown in Table 2.3. The parameters like rotational speed and tilt angle were varied during the welding, and the force, welding speed, and bed inclination angle were kept constant because of the fixed thickness of materials in each experiment. Because the Cu was positioned at the bottom with respect to the Al, there is no requirement for a backing plate during the weld. This design is superior to the previous works because it limits the deformation of the bottom portion of the Al due to the application of a large amount of force [13].

Table 2.1. Thermo-mechanical properties of the materials

	Tensile Strength	Micro-Hardness	Density	Melting temperature	Thermal Conductivity
AA1150	113 MPa	40 HV	2710 Kg/ m^3	650 °C	227 W/m-K
Oxygen-free copper	275 MPa	90 HV	8900 Kg/ m^3	1083°C	390 W/mK

The trials were conducted using a professional FSW machine manufactured by ESAB and a welding tool made of tempered H13 steel. The Selection of a welding tool was also a critical because of the hardness of the copper. Muhammad et al. used an H13 steel tool for the welding of the Al/Cu joint and received an acceptable tensile strength [14]. Hou et al. used a H13 tool steel because of its adequate hardness [15]. Similarly, many researchers have used the H13 tool for the welding of Al/Cu alloy [16–18]. A concave shoulder tool measuring 20 mm in diameter and featuring a flat tapered pin was employed for all tests. The diameter of the probe at its highest point was 4.2 mm, with a length of 4.3 mm.

Table 2.2. Condition at which samples were prepared

Sample no	***RS (RPM)***	***WS (mm/min)***	***Tilt Angle (Degree)***
S1	*640*	*160*	*3.5*
S2	*560*	*160*	*3.5*
S3	*640*	*160*	*4*
S4	*560*	*160*	*4*
S5	*640*	*160*	*4.5*
S6	*560*	*160*	*4.5*

Table 2.3. Fixed parameters during the welding

S.No.	Parameters	Value
1.	**Bed inclination angle**	8.65˚
2.	**Force**	10 kN

The machine was completely computer-controlled during the welding operation. Figure 2.1a represents the machine with a tilt angle, whereas Fig. 2.1 b represents the inclined bed. The experiments were conducted using consistent parameters, including a fixed rotational speed of 640 RPM, 160 mm/min welding speed, zero tool offset, and different tilt angles. These specific settings were determined based on prior trials. On the other hand, the appropriate force was chosen by performing the experiments initially in position control mode, and then further experiments were performed in force control mode. Different experiments were performed by keeping the Cu at the bottom position. All the experiments were performed on inclined bed conditions, as it was confirmed that it is impossible to weld the dissimilar thickness Al-Cu alloys when the top surface level gap between both materials is 3mm [13].

Samples for tensile, bending, microstructural, and macrostructural analyses were obtained by cutting perpendicular to the weld direction using a wire EDM machine. Microstructural and EBSD analyses were performed utilizing the Supra 55 FESEM machine manufactured by Carl Zeiss, Germany. Transverse tensile test specimens were derived from the welded samples and subjected to testing on a tensile testing machine in accordance with ASTM E8-16a standards (Fig. 2.1 c). XRD analysis was conducted using Panalytical X-ray diffraction equipment to identify intermetallic compounds (IMCs).

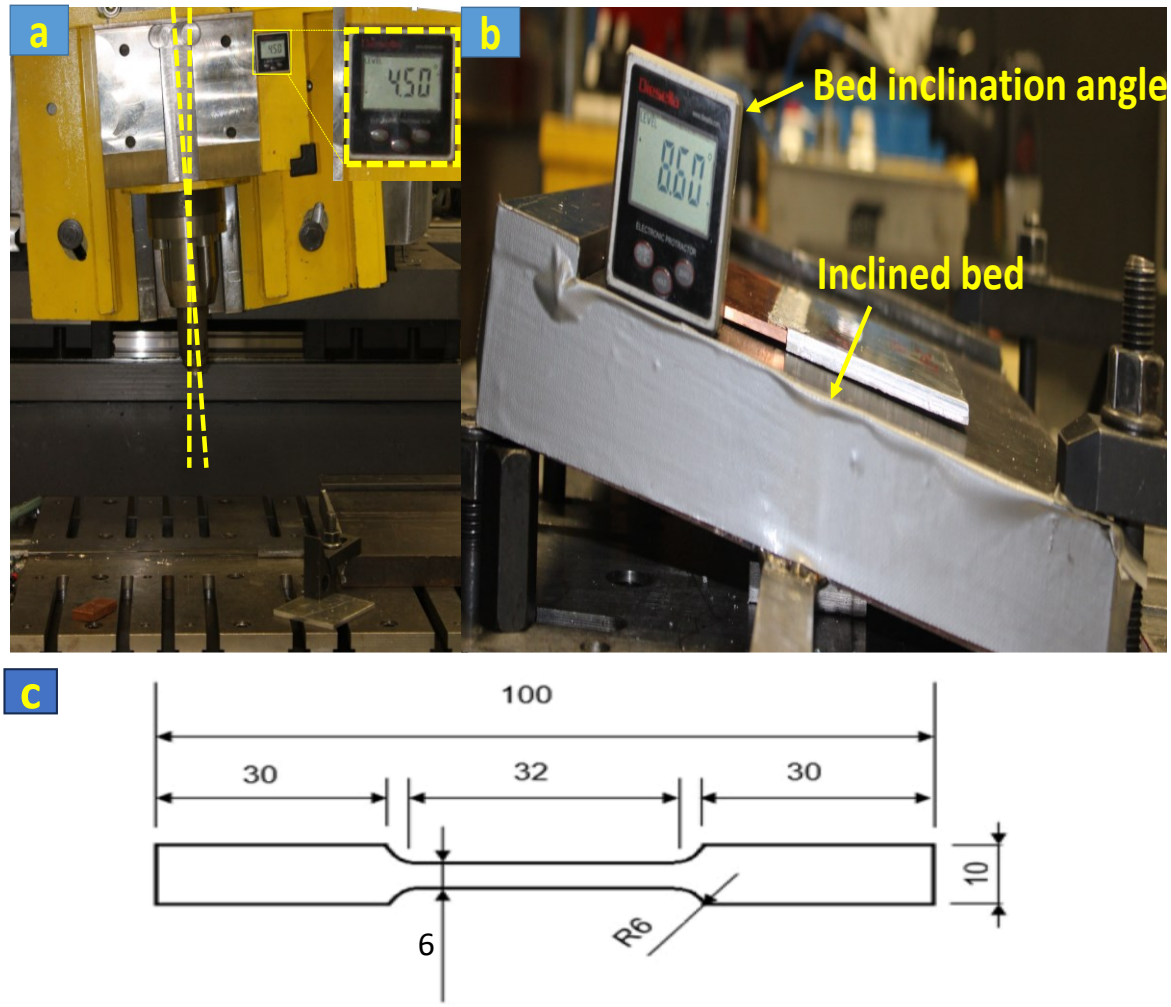

Fig. 2.1. a) Machine with tilt angle **b)** Inclined bed developed for the weld **c)** Tensile test sample dimension

2.1. Governing equation

We know that a tool tilt angle promotes a flash-free weld, while a bed inclination angle aids in achieving a uniform weld cross-section. This paper discusses the effect of tool tilt and bed inclination angles. However, we are only able to provide one of these factors at a time due to machine limitations, and the other one needs a unique bed setup. Therefore, the input parameter tilt angle has been given by the machine, and a special setup modification has been done for the bed inclination angle as it is not possible to directly define this parameter by the machine. The calculation of the exact value of the bed inclination angle is a tedious task. So, a geometric approach has been used to calculate the angle directly.

From Fig. 2.2a, it can be observed that the inclination is actually given to the bed, while during the calculation, the inclination of the shoulder with respect to the bottom plate has been calculated. Since the tool is straight during the experimentation, the only possible way is to assign the bed angle. A brief thought process leads us to conclude that the angle applied to the shoulder or the bed produces the same consequence. It is assumed that the center of the tool shoulder diameter and the center of the difference of thickness of both materials coincide together.

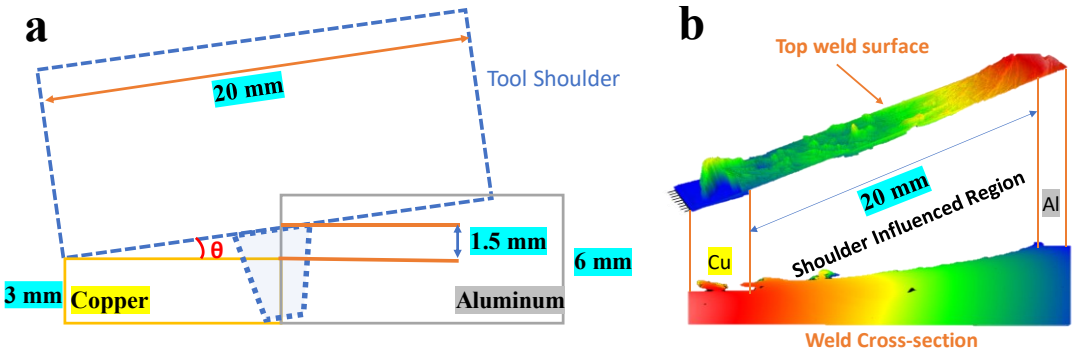

Fig. 2.2. a) Geometric approach used to calculate the bed inclination angle **b)** A uniform inclined top surface and weld cross-section after the weld

From Fig. 2.2 a, the value of Θ (bed inclination angle) can be easily calculated by the trigonometric relations.

$$\text{Sin } \Theta = \frac{Half\ of\ the\ thickness\ difference}{Radius\ of\ the\ shoulder}$$

$$\text{Sin } \Theta = \frac{1.5}{10}$$

$$\Theta = 8.62^{0}$$

Therefore, a bed inclination angle of 8.60º for all the experiments was maintained with different tilt angle combinations. The above Fig. 2.2 a represents the geometric relation between the shoulder and the uneven workpieces, whereas Fig. 2.2 b depicts the final uniform cross-section and top of the weld surface.

3. Results and Discussions

3.1. Macro-structural and microstructural analysis

The inclination of the tool axis significantly influences the excess material flow and flash formation during the FSW process. During the FSW process, the tool axis was frequently tilted at an angle relative to the typical workpiece surface. An optimal tool tilt towards the trailing side enabled the shoulder to effectively retain the stirred material and convey it from the leading side to the trailing side.. Li et al. [19] introduced a plastic material flow model for FSW, drawing from their experimental findings and existing literature, which delineated distinct flow patterns vertically and elucidated the emergence of excess material flow. Figure 3.1 illustrates a conceptual model aiding in comprehending excess material flow formation. In this conceptual framework, the angled shoulder was firmly affixed to the workpiece, exerting a diagonal downward pressure. This force could be dissected into two elements: a forward thrust and a downward push. The forward thrust facilitated the movement of stirred material into the concave of the shoulder, thereby preventing the formation of flash and contributing to a refined weld surface appearance. Conversely, the downward push from the advancing side directed the plastic material flow deeper into the Weld Nugget Zone (WNZ), complemented by the rotational motion of the shoulder.

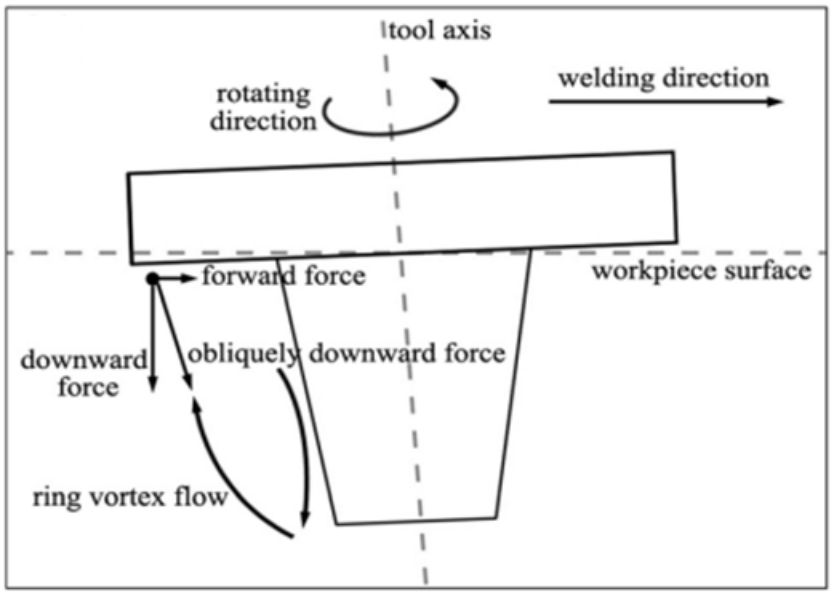

Fig. 3.1. Relation between tool tilt angle and vertical force [19]

Surface morphologies and weld cross-sections of different welds under varied conditions are depicted in Fig. 3.2. and Fig 3.3. Since the top surface of the weld is dominated by the aluminum alloy, the chances of flash formation increase because of its superior flowability. The purpose of the different tilt angles is to reduce the flash formation. Visual inspection was used to assess the weld surface quality of welded plates, whereas macro investigation was used to identify interior issues. At a tilt angle of 3.5˚, the excessive flash effect was observed. Furthermore, the flash effect is reduced as the tilt angle increases from 3.5 to 4.5˚. The rise in heat input and compressive force was responsible for this[20][21]. As the tool tilt angle increases, the axial plunge load value increases, pushing the material downward and preventing it from spreading outside. Fig. 3.2. shows a flash formation reduction with the tool tilt angle increase. Each sample prepared at a tilt angle of 3.5˚ shows a higher flash formation than the higher tilt angles. On the other hand, samples, S5 and S6, which are prepared at 4.5˚, show an almost flash-free weld. The flash formation in the case of S3 and S4, which is prepared at 4˚, is between 3.5˚ and 4.5˚. However, these flashes are of a soft nature and can be removed by a hand tool.

However, the surface of every weld is defect-free because of the excessive available Al alloy. The low value of the axial plunge load at a smaller tilt angle leads to the uneven distribution of materials on the top surface. Samples S1, S3 & S5 are prepared at a rotational speed of 640 RPM, whereas samples S2, S4 & S6 are prepared at a rotational speed of 560 RPM. Since the rotational speed of 640 RPM produces more heat comparatively, therefore, the chances of uneven material distribution on the top of the surface are higher. Welded surfaces prepared at higher rotational speeds have a darker look, whereas weld surfaces produced at lower rotational speeds have a comparably lighter surface appearance. The appearance of the surfaces varies due to the hot and cold weld circumstances. Like surface appearance, flash formation is also an issue in dissimilar FSW of Cu and Al. However, the problem becomes more complicated because of Al's excessive participation in the weld zone. The shoulder of the tool rotates the material in contact and forces it downward and thus resulting in vortex flow.

The weld zone of different samples is shown in Fig. 3.3. The most noteworthy discovery of this joining method is that all samples, regardless of weld input parameters or surface appearance, result in a sound and defect-free weld. The top part of the weld zone is more uniform and aligned in the case of 560 RPM rotational speed, as shown in Fig 3.3 b, Fig 3.3 d, and Fig 3.3 f, which is confirmed by samples S2, S4, and S6. On the other hand, samples S1,

S3, and S5 show an uneven deposition of materials on the top of the weld surfaces, which are prepared at 640 RPM rotational speed. In both settings, two types of weld zones are achieved. Because the tool pierces the workpiece at an angle, it scrapes the copper and mixes it in the weld zone. Because a reduced tool tilt angle minimizes weld force, material mixing in the weld zone is essentially non-existent as shown in Fig 3.3 a and 3.3 b. However, in case of increasing the tool tilt angle to 4˚ leads to better material mixing and widened weld zone compared to the initial welds prepared at tool offsets of 3.5˚. A similar type of trend is also followed by the samples S5 and S6, which were prepared at a tilt angle of 4.5˚. Besides the material mixing and fragmentation, hooking is an additional feature which was observed in the S5 and S6. This hooking structure also plays a great role in mechanical interlocking, as suggested by Li et al. [22]. The hook structure lengthened the joint interface and increased mechanical interlocking at the joint bottom, delaying fracture propagation under tensile load [23].

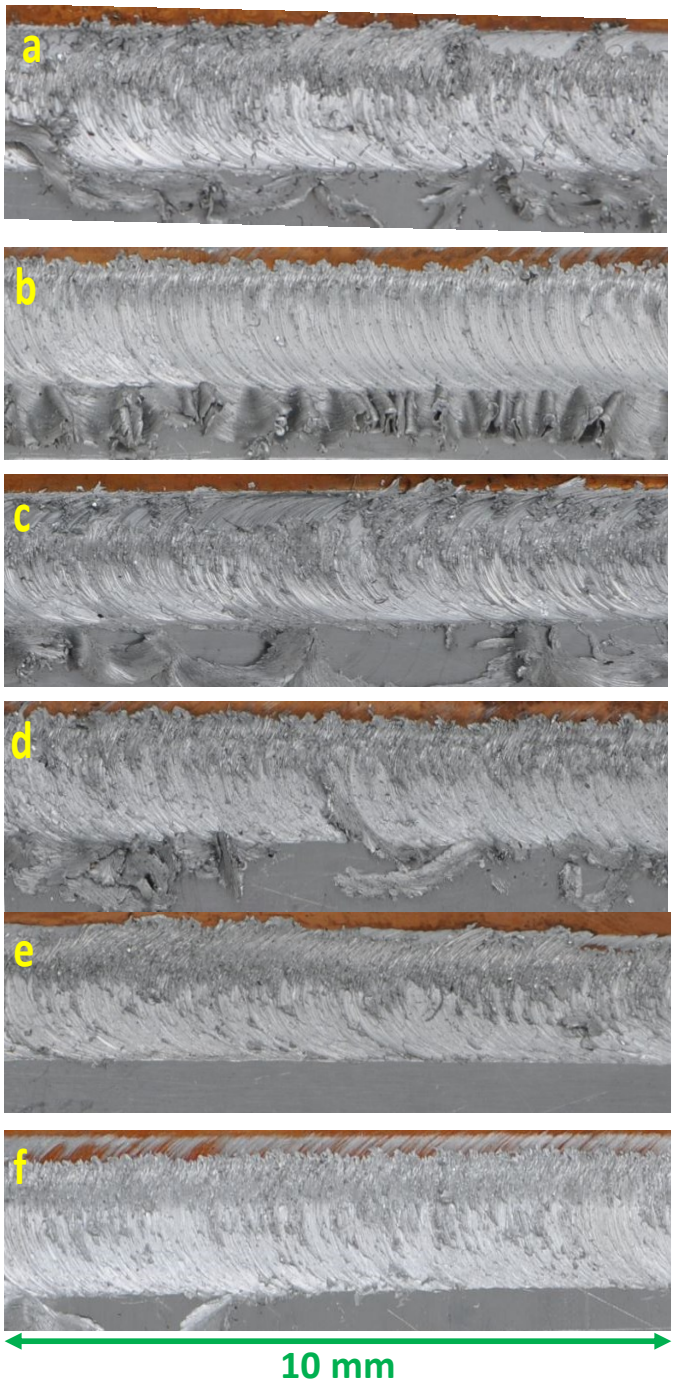

Fig. 3.2. *Surface morphologies of a) S1 b) S2 c) S3 d) S4 e) S5 f) S6*

Various flow patterns emerge during the FSW of Cu and Al, manifesting within the blended area of the weld zone., as shown in Fig. 3.4. The most common feature of the weld zone is a circular structure similar to the onion ring, which forms due to the circular movement of Cu and Al in the root, as shown in Fig. 3.4 a. Under an optical microscope, one can observe these bands, which typically exhibit concentric circular or circular shapes in the transverse plane of

the weld. The vortex flow of the material causes Cu pieces to migrate downward, and due to the high plunging force, the copper material is changed into a ring structure. When a higher proportion of copper is available at the root, the probabilities of a multi-ring structure (see Fig. 3.4 a), also known as an onion ring structure, at the bottom increases, whereas a single or double circle ring structure is obtained when the fraction of copper at the root is low (See in Fig. 3.4 b). Besides the onion ring, the lamellar or layered structure is also a common feature in the FSW of Cu and Al. In contrast to the FSW of homogeneous materials, intercalation is a common structure observed across the WN that involves lamellar alternating patterns. Furthermore, identical lamellar alternating structures of stacked Cu and Al can be found throughout the mixed area of the weld nugget zone.

These lamellar structures are also called layered structures, consisting of an alternate layer of aluminum and copper alloys. These layered structures can be classified into bulky copper layered structures (See Fig. 3.4 c, 3.4 d) and fine copper layered structures (see Fig. 3.4 d). A bulky copper layered structure can be easily observed by an optical microscope, whereas the finer one is obtained by scanning electron microscope. In addition to the above-mentioned structure, composite structure (see in Fig. 3.4 d) is one of the most common structures in FSW of aluminum and copper, greatly enhancing the mechanical property of the friction stir welded joints.

The finer distribution of copper in the weld zone is analyzed at higher magnification by FESEM. As discussed above, an elevation in the tool tilt angle increases the intensity of force, leading to a corresponding heat input increase. As shown in Fig. 3.5 a & 3.5 b, there is a lack of material mixing at a lower tilt angle, irrespective of the rotational speed; however, it increases with the increment in tilt angle. With a tilt angle of 3.5˚, most of the copper is in the form of bulky copper fragments. These bulky copper particles break into the mixture of finer and bulky particles at a 4˚ tilt angle. On the other hand, these copper particles are sub-divided into completely finer particles at 4.5˚. Tilt angle is not the only parameter affecting material mixing; rotational speed also plays a significant role in mixing materials in the weld zone. The effect of rotational speed can be easily identified in Fig 3.5 c & 3.5 e, which is prepared at 640 RPM. The distribution of the Al-Cu mixed zone is more uniform in samples S3 and S5 (see Fig 3.5 c & 3.5 e) than S4 and S6 (see Fig 3.5 d & 3.5 f). The weld SZ has a composite structure with Al as the matrix and copper pieces as the secondary phase [24].

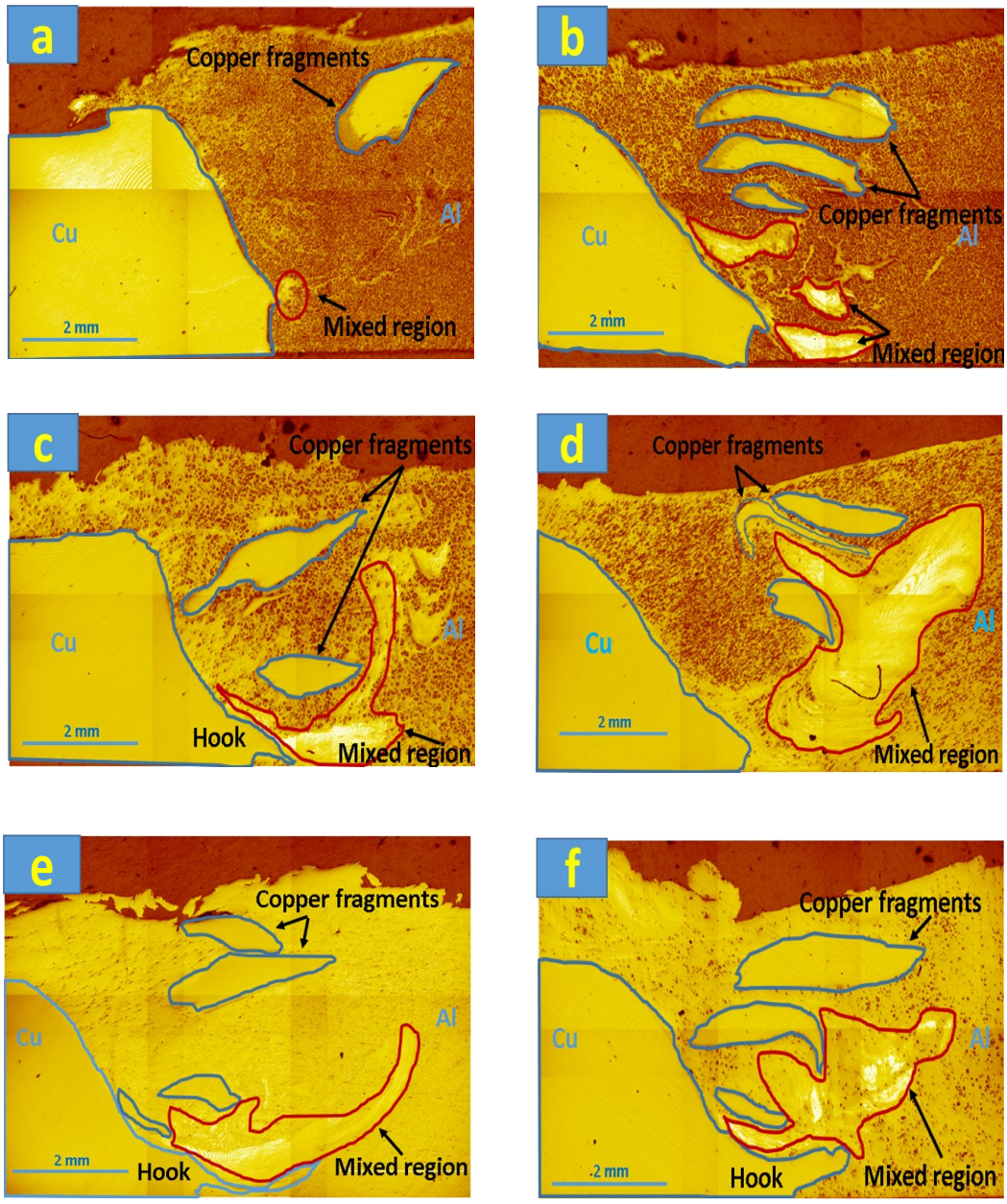

Fig. 3.3. *Cross-sectional image of the different welds a) S1 b) S2 c) S3 d) S4 e) S5 f) S6*

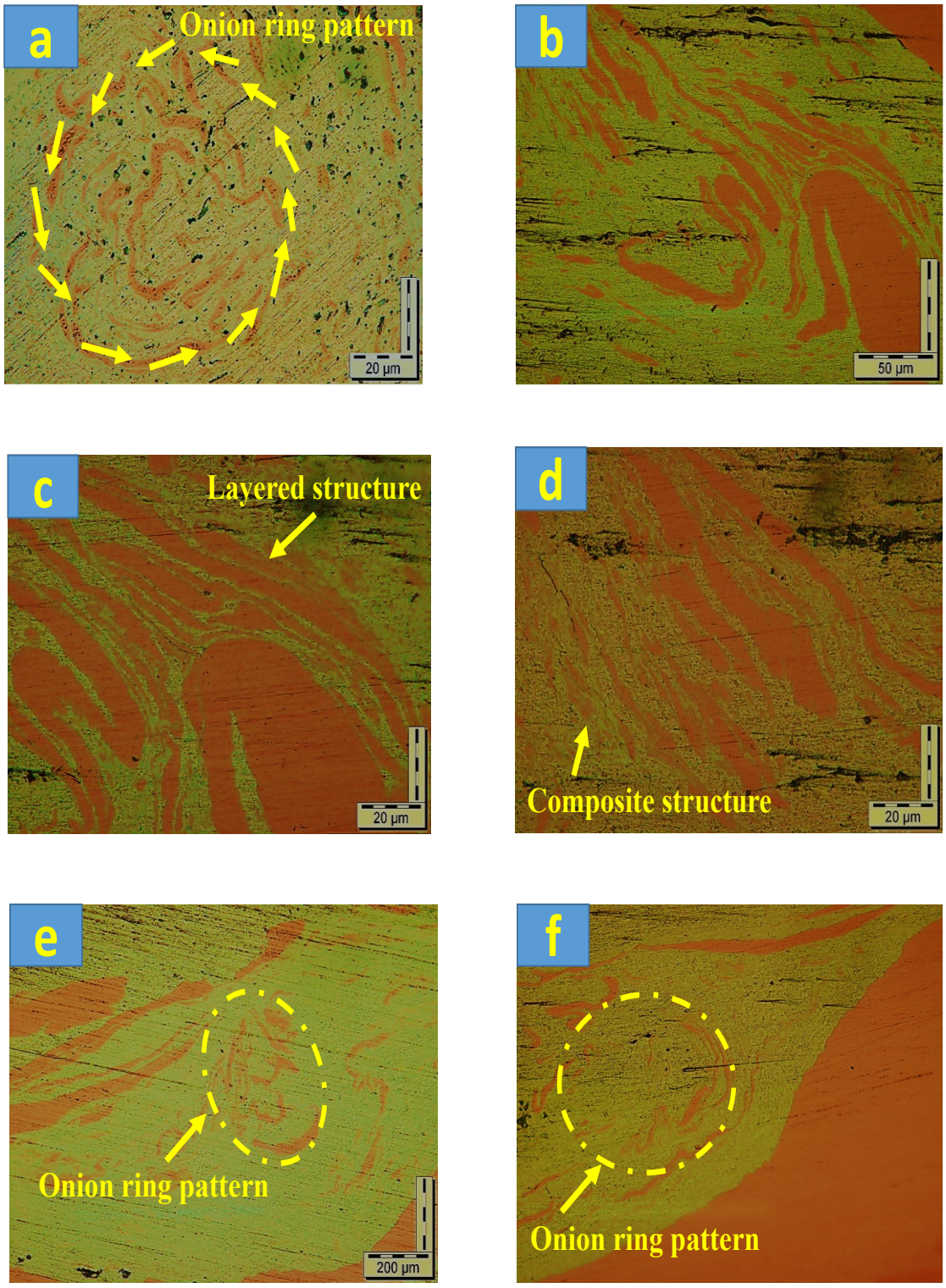

Fig. 3.4. *Different types of flow structures observed in the weld zone*

The 640 RPM rotational speed produces additional heat than the 560 RPM and thus leads to the softening of the copper material. Simultaneously, rising pressure with increasing tilt angle compacts the materials in the weld zone, resulting in a composite-like structure in the weld

zone and improved mechanical properties. Almost all welds are defect-free because of the improved flowability of the Al alloy. Increased tool tilt angle enhances the flow properties of the stir zone material, allowing the weld material to fill the defects more effectively. As the thermal conductivity of Al is lower than that of Cu, the thermal softening of Al will be greater.

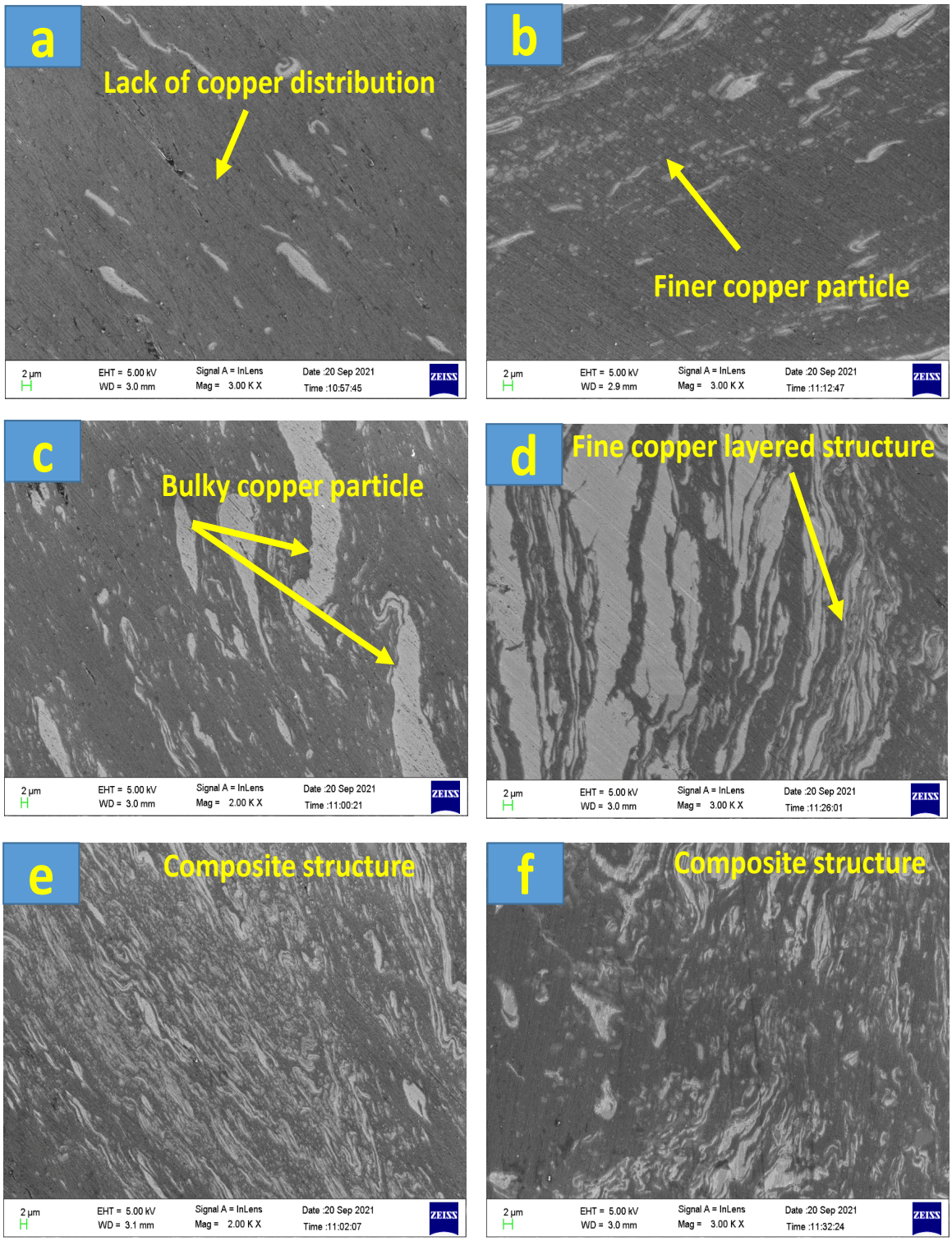

Fig. 3.5. *Distribution of Cu in the weld zone*

The IPF map and grain size distribution of the weld stir zone, and the interfacial zone are shown in Fig 3.6. A very refined grain is obtained in the weld stir zone. The substantial plastic deformation and heat input from the rotating tool significantly affect the microstructural changes occurring within the stir zone (SZ). The continuous strain induces dislocation glide, resulting in the gradual relative rotation of neighboring sub-grains within the initial grains characterized by low-angle boundaries [25]. The concurrent presence of elevated temperatures and sustained plastic deformation fosters the ongoing rotation of sub-grains, ultimately leading to the conversion of low-angle grain boundaries into High-Angle Grain Boundaries (HAGBs). The average grain size of the Al base metal was 22.25 μm, which is reduced to 11.84 μm (See Fig. 3.7 d) after the FSW process in the stir zone. This grain refinement was due to heat generation and continuous plastic deformation. A completely different type of grain was obtained at the interfacial region of the weld zone and Cu base metal. The average grain size of that region was reduced to 1.78 μm (See Fig. 3.7 a). The interfacial region of the weld was experiencing cyclic deformation due to the continuous rotation of the pin. It thus resulted in a completely different type of grain than in the stir zone. This type of grain is due to the complete recrystallization of the material. For clarity, the interfacial region analysis was performed at higher magnification, which reveals the intermetallic layer thickness. Fig 3.6 b & 3.6 e represent the misorientation angle of the interfacial region and the stir zone. In the case of the interfacial region, the maximum fraction of grains has shown a misorientation angle between (0˚-10˚), which can also be confirmed by the boundary rotation angle map (Fig. 3.7 c). 70.3% of grains have shown a rotation angle between 1˚-5˚ whereas 12.5% have presented a rotation angle of 5˚-15˚. Since the grains between 1˚ to 15˚ are considered low-angle grain boundaries (LAGBs), the total fraction of low-angle grain boundaries is 83.5%, which manifests the dominance of LAGBs compared to high-angle grain boundaries (only 17.2%). The interfacial area of the Cu material is not in direct contact with a pin. As a result, this area undergoes significant deformation solely due to the repetitive impact of the tool probe. However, the grain boundary rotation angle situation is entirely different in the stir zone compared to the interfacial region. Since the WZ material is in direct contact with the pin, most LAGBs are transformed into HAGBs. The total fraction of HAGBs in the stir zone region is 43.5% (Fig 3.7 f), which is

higher than that of Al base alloys (17.2% HAGBs only) (Fig 3.7). The grain misorientation shows a variety of misorientation angle fractions (Fig 3.7 e).

The weld stir zone introduces the grain refinement and shows an intermetallic layer at the weld zone-Cu interface. XRD test was performed to analyze this intermetallic layer and the Al-Cu mixed zone of the samples S5 and S6, respectively (Fig. 3.6 e). The three primary intermetallic compounds produced in the weld zone are Al_2Cu, AlCu, and Al_4Cu_9. Al_2Cu phases emerge at a temperature of 150˚C, whereas Al_4Cu_9 phases are generated at 350˚C. The bond strength diminishes rapidly when the intermetallic phase reaches a thickness of 10 μm. Enhanced swirling and mixing of the bulk Cu particles resulted in the formation of intermetallic compounds within the weld zone, as no offsets were employed. Among the various reasons, the production of intermetallic is one that leads to the reduction of joint strength in Al-Cu dissimilar FSW. These intermetallic compounds are hidden elements that restrict joint strength from reaching the level of aluminum's strength [26].

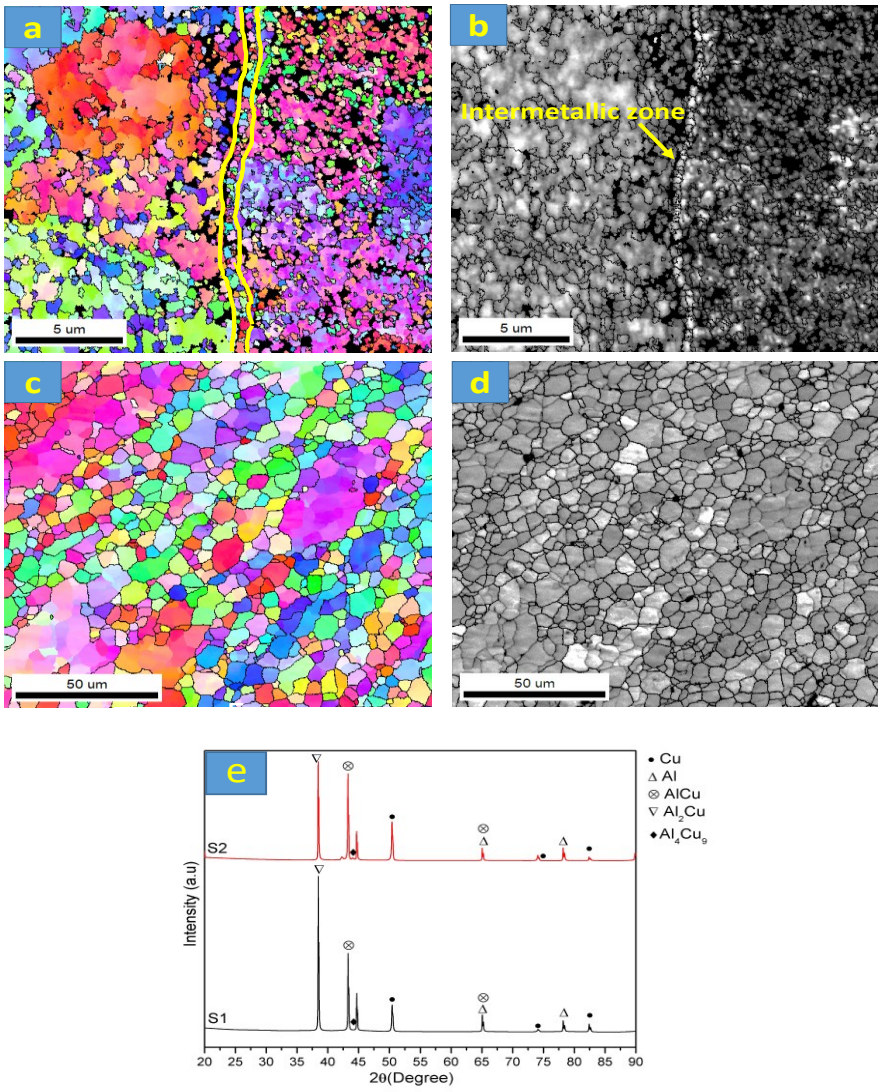

Fig. 3.6. a),b) *EBSD mapping of Cu-WZ interface area* ***c),d)*** *Refined grains of WN* ***e)*** *XRD analysis*

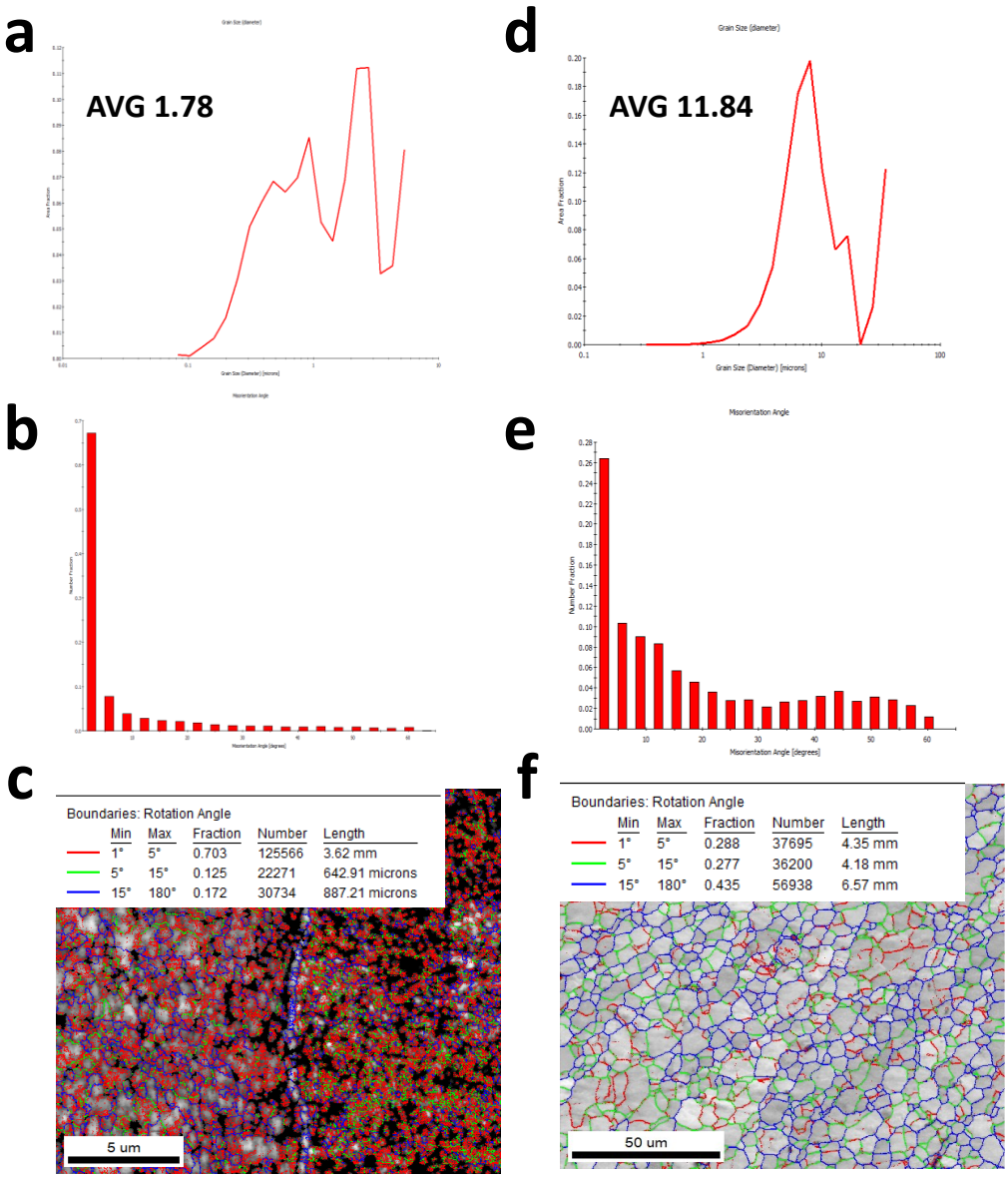

Fig. 3.7. *a) Grain size diameter of interfacial region b) grain orientation angle of interfacial region c) boundaries rotation angle of interfacial region d) grain size diameter of stir zone e) grain orientation angle of stir zone f) Boundary rotation angle of stir zone*

3.2.Tensile strength of the welds

The tensile tests conducted on various samples, as depicted in Fig. 3.8a, reveal distinct performances based on their preparation conditions. A total of three tensile test specimens were tested from each sample. Fig. 3.8 b illustrates the joint efficiency of welds compared to the base aluminum (Al) alloy. Dissimilar weld strength is consistently assessed relative to the weakest base metal. Sample S6, comprising 96.38% Al base metal (113 MPa), achieved the highest tensile strength at 108.91 MPa. Conversely, sample S1, with 88.56% Al base metal, recorded the lowest tensile strength at 100.08 MPa. Fig. 3.8 confirms that the tensile strength gets enhanced with the increase in tilt angle. The tilt angle increases the material mixing and widens the stir zone, enhancing the joint's mechanical properties.

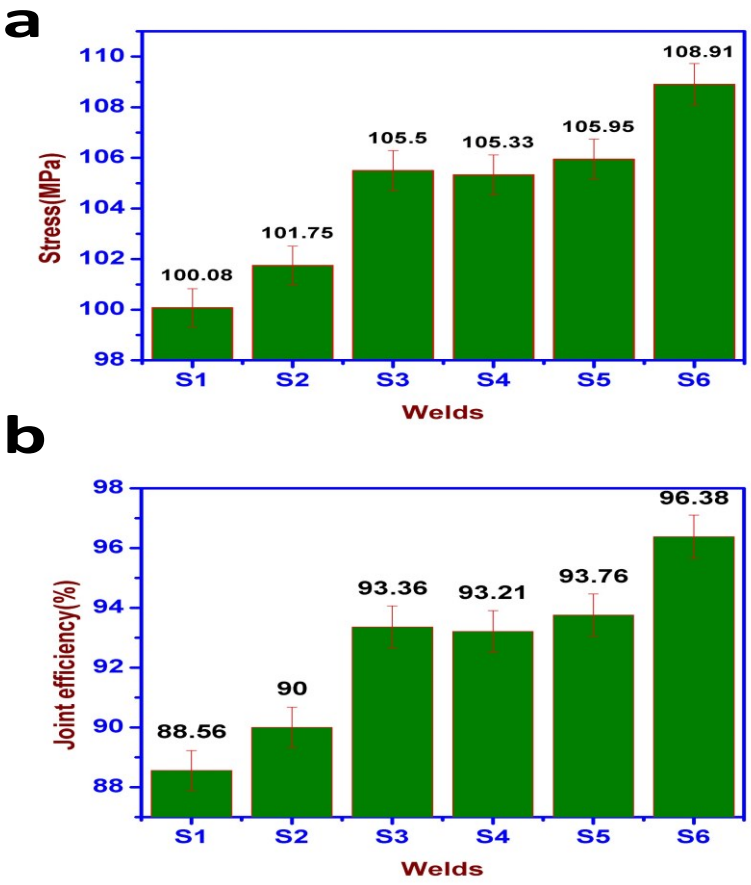

Fig. 3.8. *a) UTS of different welds b) Joint efficiency compared to Al base metal*

Both welds S1 and S2, prepared at a lower tilt angle of 3.5˚, show a tensile strength of 88.56% and 90% compared to the base Al alloy, which is equivalent to the maximum tensile strength

of 101.45 MPa obtained with the offsets of one mm [12]. Hooking formed at the root of the weld with the material mixing has also influenced the tensile strength. Welds S3, S5, and S6 have revealed a decent tensile strength because of the hook's formation at the weld's root. On the other hand, Weld S4 has shown improved weld quality because of the decent material mixing. However, in terms of combined parametric effects such as minimum flash formation, proper material mixing, wider weld stir zone, and improved tensile strength of both the welds S5 and S6 have shown a sound weld quality as well as flash free surface. However, weld S6 has shown better strength than the S5. Despite the decent material mixing and defect-free weld, the maximum possible joint efficiency with the above parameter was 96.38%, which is 3.62% less than the 100% joint efficiency. The only possible cause for the reduction in joint efficiency is the formation of intermetallics.

The tensile testing of Al/Cu joints involved investigating their deformation behavior, as illustrated in Fig. 3.9. This investigation utilized a 2D digital image correlation (DIC) technique within the speckled region shown in the larger specimen image. The distribution and development of major principal strain along the Stir Zone (SZ) region and its adjacent areas in Friction Stir Welding (FSW) joints were documented. Three samples, each representing a different tilt angle, were selected for DIC analysis.

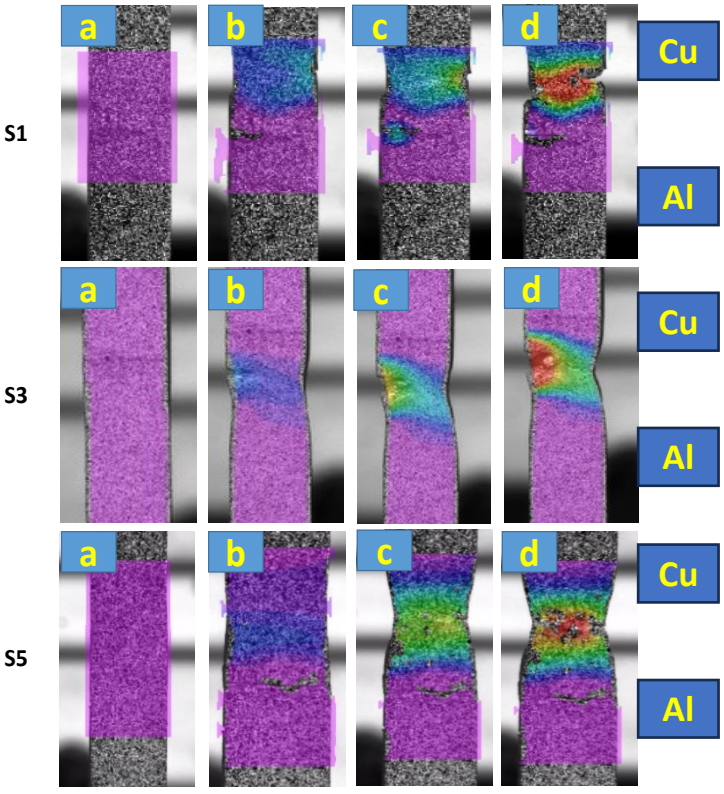

Fig. 3.9. *Fracture pattern of samples S1, S3, S5 using DIC*

The measurement can also determine the fracture processes and behavior following each joint's failures. Fracture progression in all samples commences once the specimen undergoes stress and initial deformation, leading to strain development, crack initiation, and propagation. The joint failure occurred swiftly, primarily attributed to minimal or negligible plastic deformation observed in sample S1. The fracture resembles a brittle fracture. In sample S3, the specimen's right side shows more deformation than the left. However, the fracture is more ductile than that of the sample S1. Unlike the S1 and S3, sample S5 manifests more elongation and ductility in the weld zone.

3.3.Fracture surface analysis

Fig. 3.9 shows the microstructures of the failure zones and the SEM micrograph. The dominant failure mode was ductile in nature with fine dimples. However, varied fracture surfaces were obtained with different samples. Almost all figures except Fig. 3.10 d show the complete ductile fracture. There are variations in the dimples' size, shape, and direction. The Fig. 3.10 d was comparatively captured at low magnification, which reports a mixture of flat and ductile surfaces. It is evident from the figures that a fractured surface cannot be completely ductile, irrespective of the degree of mixing. Fig 3.10 a, b, c, e, f shows the magnified images of the different ductile surfaces. Fig. 3.10 a shows the shallow dimples, which confirm lower energy before fracture. On the other hand, Fig. 3.10 c shows the deep and equiaxed samples elongated along the loading direction, indicating greater energy before fracture.

Different from Fig. 3.10 c & e, fig 3.10 b shows a different variety of dimples with some flat surfaces in the weld zone, which are indicative of moderate force values prior to fracture. Tearing ridges and deep dimples are also a feature of ductile failures [27]. These ridges are common in Fig. 3.10 b, e & f, whereas ridges are absent in Fig. 3.10 a, representing shallow dimples. However, these ridges are absent in equiaxed and elongated dimples of Fig. 3.10 c claims that the ridges are not the only feature of ductile failure. Fig 3.11 represents the failure locations of each weld from the welded cross-section and top parts of the welds. Two different types of fracture locations were observed: fracture at the stir zone and fracture from the thermo-mechanically affected zone along the Al side. Only samples S1 and S2 were fractured at the stir zone; on the other hand, the rest of the samples were fractured at TMAZ along the Al side.

Muthu and Jayabalan also observed the maximum tensile strength of 104MPa when the fracture location was TMAZ along the Al side in FSW of Al-Cu alloys.

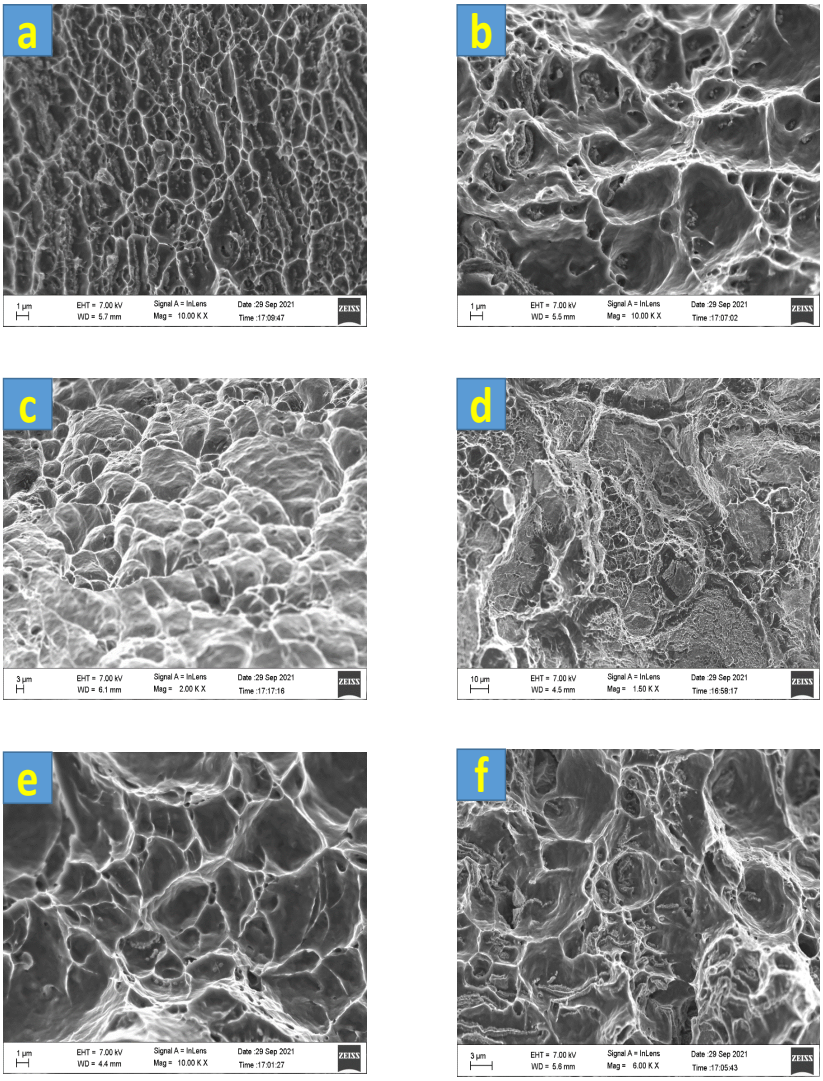

Fig. 3.10. *Different type of fracture surfaces a) S1 b) S2 c) S6 d) S1 e) S6 f) S1*

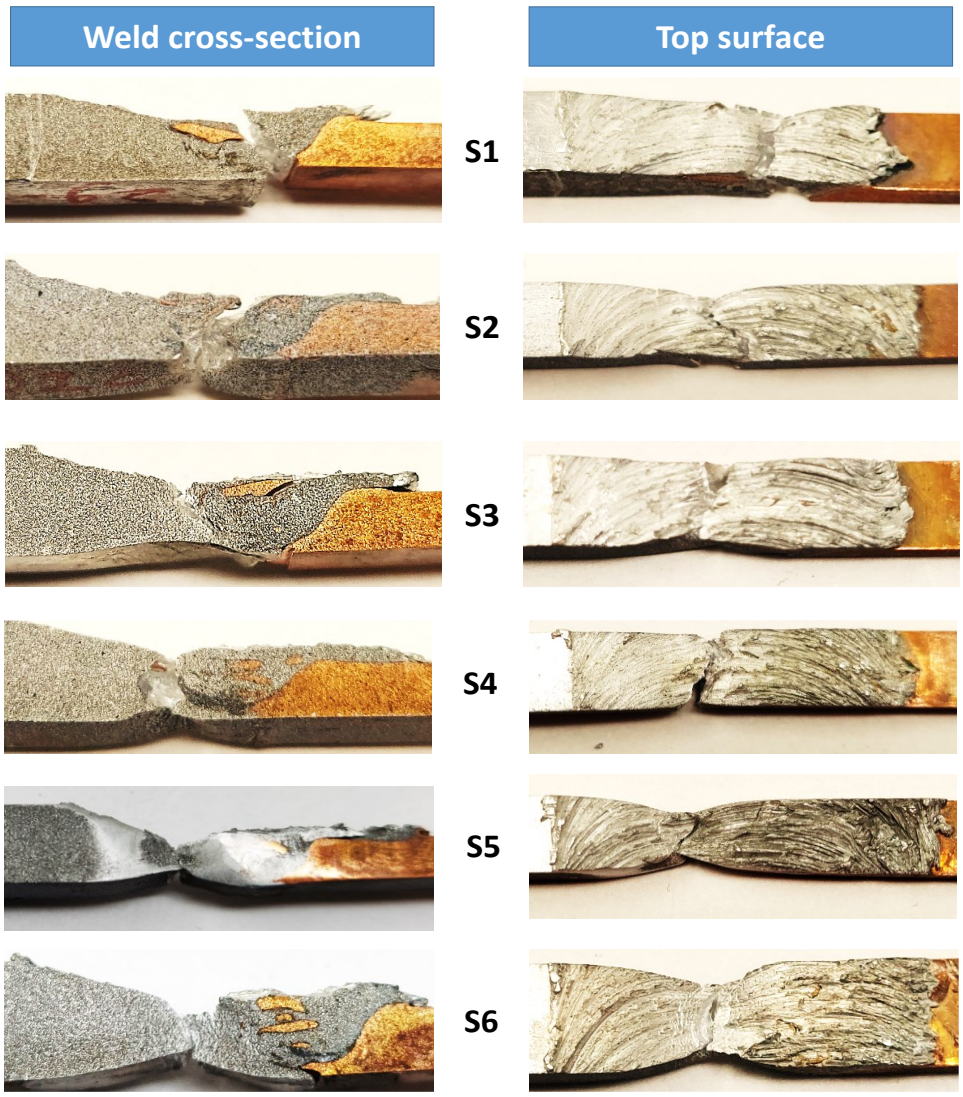

Fig. 3.11. *Fracture locations of different welds*

3.4.Micro-hardness analysis

The micro-hardness distribution within sample S6 was analyzed along the central section of the transverse cross-section, depicted in Fig. 3.12. While the base Al alloy exhibited an average micro-hardness of 40HV and Cu showed an average of 90HV, the weld zone displayed varying micro-hardness levels, indicating an uneven distribution of Cu particles within the weld nugget. These Cu particles were observed in both fine and coarse forms. The highest hardness of 152.26 HV was recorded in the weld nugget, attributed to the presence of Al solid solution and intermetallic compounds (IMCs) within the mixed layer, making it the hardest region across the cross-section. Conversely, the minimum micro-hardness, ranging between 33.57-34.25HV,

was observed at the extreme ends toward the Al alloys. This decrease in hardness suggests the presence of Heat HAZ along the Al alloy, resulting from the dissolution of precipitates.

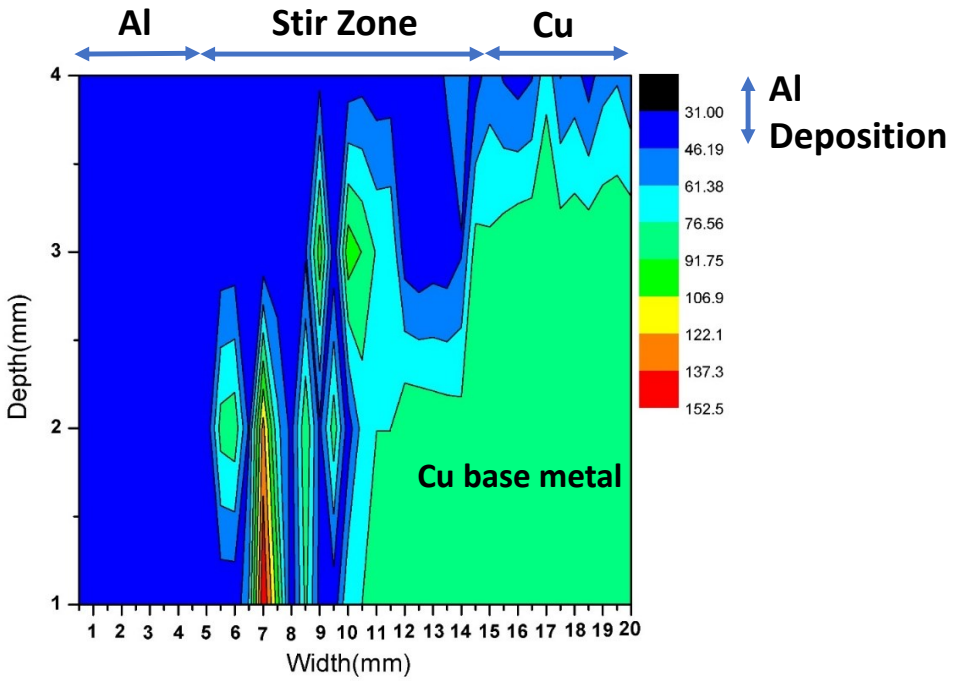

Fig. 3.12. *Micro-hardness distribution of Al-Cu FSWed specimen*

3.5.Three-point bending test analysis

Fig. 3.13 illustrates the macroscopic examination of root bend specimens subjected to a three-point bending test, focusing on samples S5 and S6. The weld metal exhibits notable plastic deformation and root surface cracks extending toward the weld nugget zone. Since samples S5 and S6 demonstrated the highest joint strengths at 105.95 MPa and 108.91 MPa, respectively, they were exclusively chosen for the root bend test. The lower segment of the bent samples experiences tensile forces, while the upper part undergoes compressive forces. Both samples exhibit maximum bending angles of 107 degrees.

As Al is the dominant element in both samples, its superior ductility has resulted in an enhanced bending angle. The bottom end of both the alloys, Cu and Al are at the same level, resulting in abundant joint failures during the test.

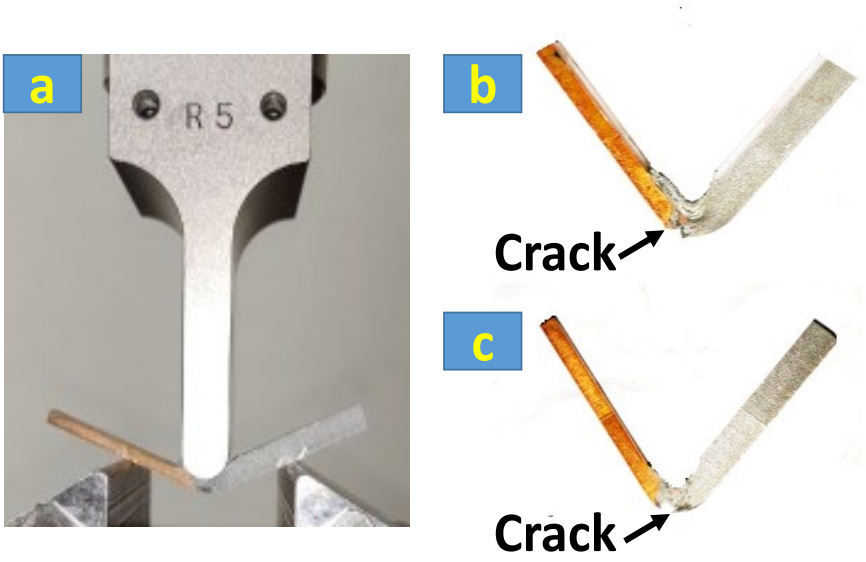

Fig. 3.13. *a) Three-point bend test of Al-Cu FSWed specimen b) S5 and c) S6*

4. Conclusions

1. Dissimilar thickness Al-Cu alloys were successfully welded by FSW when the differences in the level of both the materials are 3 mm. The bed inclination angle ensured decent locking of the materials under the shoulder. In contrast, the tilt angle helped maintain the additional Al alloy under the shoulder and thus resulted in a uniform and flash-less cross-section.

2. The increment in tool tilt angle reduces the flash formation during the FSW process. This increment in tool tilt angle lifts the front part of the tool shoulder and provide enough space for the excess material to get settled in the weld zone.

3. Sample S6 achieved the highest tensile strength at 108.91 MPa, representing 96.38% of the base Al alloy, while the lowest strength of 100 MPa was recorded in sample S1. The reason behind the maximum strength lies in the effective mixing of materials and the absence of defects in the joints.

4. Samples S5 and S6 exhibit a bending angle of 107 degrees in the three-point bending test, indicating that they possess the highest tensile strength and the most favorable bending angle.

5. The Heat Affected Zone (HAZ) adjacent to the aluminum side exhibited the lowest micro-hardness at 33.57 HV, while the Al-Cu mixed zone displayed the highest micro-hardness at 152.26 HV. This improved hardness is attributed to the presence of intermetallic compounds formed within the mixed region. Among the intermetallics commonly generated in the weld zone are AlCu, Al2Cu, and Al4Cu9.

References

[1] M.B. Senior, N. Alexandrov, Intermetallic Compounds at Aluminum-to-Copper Electrical Interfaces: Effect of Temperature and Electric Current, 1994.

[2] Z.L. Ni, F.X. Ye, Dissimilar Joining of Aluminum to Copper Using Ultrasonic Welding, Materials and Manufacturing Processes 31 (2016) 2091–2100. https://doi.org/10.1080/10426914.2016.1221101.

[3] S. Shankar, K.P. Mehta, S. Chattopadhyaya, P. Vilaça, Dissimilar friction stir welding of Al to non-Al metallic materials: An overview, Mater Chem Phys 288 (2022). https://doi.org/10.1016/j.matchemphys.2022.126371.

[4] S. Emami, T. Saeid, A comparative study on the microstructure development of friction stir welded 304 austenitic, 430 ferritic, and 2205 duplex stainless steels, Mater Chem Phys 237 (2019). https://doi.org/10.1016/j.matchemphys.2019.121833.

[5] N.D. Nam, L.T. Dai, M. Mathesh, M.Z. Bian, V.T.H. Thu, Role of friction stir welding - Traveling speed in enhancing the corrosion resistance of aluminum alloy, Mater Chem Phys 173 (2016) 7–11. https://doi.org/10.1016/j.matchemphys.2016.02.004.

[6] C. Zhou, X. Yang, G. Luan, Investigation of microstructures and fatigue properties of friction stir welded Al-Mg alloy, Mater Chem Phys 98 (2006) 285–290. https://doi.org/10.1016/j.matchemphys.2005.09.019.

[7] E. Cerri, P. Leo, Aging of medium strength aluminum alloy friction stir welds produced by different process parameter after tensile strain hardening, Mater Chem Phys 147 (2014) 1123–1133. https://doi.org/10.1016/j.matchemphys.2014.06.068.

[8] A. Tamadon, A. Baghestani, M.E. Bajgholi, Influence of WC-Based Pin Tool Profile on Microstructure and Mechanical Properties of AA1100 FSW Welds, Technologies (Basel) 8 (2020). https://doi.org/10.3390/technologies8020034.

[9] N. Dialami, M. Cervera, M. Chiumenti, Defect formation and material flow in Friction Stir Welding, European Journal of Mechanics, A/Solids 80 (2020). https://doi.org/10.1016/j.euromechsol.2019.103912.

[10] S. Shankar, S. Chattopadhyaya, K.P. Mehta, P. Vilaça, Influence of copper plate positioning, zero tool offset, and bed conditions in friction stir welding of dissimilar Al-Cu alloys with different thicknesses, CIRP J Manuf Sci Technol 38 (2022) 73–83. https://doi.org/10.1016/j.cirpj.2022.04.001.

[11] P. Vilaça, J.P. Santos, A. Góis, L. Quintino, Joining aluminium alloys dissimilar in thickness by friction stir welding and fusion processes, Welding in the World 49 (2005) 56–62. https://doi.org/10.1007/BF03266476.

[12] S. Shankar, P. Vilaça, P. Dash, S. Chattopadhyaya, S. Hloch, Joint strength evaluation of friction stir welded Al-Cu dissimilar alloys, Measurement (Lond) 146 (2019). https://doi.org/10.1016/j.measurement.2019.07.019.

[13] S. Shankar, S. Chattopadhyaya, K.P. Mehta, P. Vilaça, Influence of copper plate positioning, zero tool offset, and bed conditions in friction stir welding of dissimilar Al-Cu alloys with different thicknesses, CIRP J Manuf Sci Technol 38 (2022). https://doi.org/10.1016/j.cirpj.2022.04.001.

[14] N.A. Muhammad, C.S. Wu, H. Su, Concurrent influences of tool offset and ultrasonic vibration on the joint quality and performance of dissimilar Al/Cu friction stir welds, Journal of Materials Research and Technology 14 (2021) 1035–1051. https://doi.org/10.1016/j.jmrt.2021.07.009.

[15] W. Hou, Z. Shen, N. Huda, M. Oheil, Y. Shen, H. Jahed, A.P. Gerlich, Enhancing metallurgical and mechanical properties of friction stir butt welded joints of Al–Cu via cold sprayed Ni interlayer, Materials Science and Engineering: A 809 (2021). https://doi.org/10.1016/j.msea.2021.140992.

[16] A. Mahdianikhotbesara, M.H. Sehhat, M. Hadad, Experimental Study on Micro-Friction Stir Welding of Dissimilar Butt Joints Between Al 1050 and Pure Copper, Metallography, Microstructure, and Analysis 10 (2021) 458–473. https://doi.org/10.1007/s13632-021-00771-5.

[17] J. You, Y. Zhao, C. Dong, S. Miao, Z. Liu, L. Liu, Y. Su, Microstructural evolution and mechanical properties of the Al–Cu dissimilar joint enhanced by stationary-dynamic shoulder friction stir welding, J Mater Process Technol 300 (2022). https://doi.org/10.1016/j.jmatprotec.2021.117402.

[18] R. Khajeh, H.R. Jafarian, S.H. Seyedein, R. Jabraeili, A.R. Eivani, N. Park, Y. Kim, A. Heidarzadeh, Microstructure, mechanical and electrical properties of dissimilar friction stir welded 2024 aluminum alloy and copper joints, Journal of Materials Research and Technology 14 (2021) 1945–1957. https://doi.org/10.1016/j.jmrt.2021.07.058.

[19] Y. Huang, Y. Wang, L. Wan, H. Liu, J. Shen, J.F. dos Santos, L. Zhou, J. Feng, Material-flow behavior during friction-stir welding of 6082-T6 aluminum alloy, International Journal of Advanced Manufacturing Technology 87 (2016) 1115–1123. https://doi.org/10.1007/s00170-016-8603-7.

[20] R. Nandan, T. DebRoy, H.K.D.H. Bhadeshia, Recent advances in friction-stir welding - Process, weldment structure and properties, Prog Mater Sci 53 (2008) 980–1023. https://doi.org/10.1016/j.pmatsci.2008.05.001.

[21] N. Muhayat, A. Zubaydi, Sulistijono, M.Z. Yuliadi, Effect of tool tilt angle and tool plunge depth on mechanical properties of friction stir welded AA 5083 joints, Applied Mechanics and Materials 493 (2014) 709–714. https://doi.org/10.4028/www.scientific.net/AMM.493.709.

[22] B. Li, Z. Zhang, Y. Shen, W. Hu, L. Luo, Dissimilar friction stir welding of Ti – 6Al – 4V alloy and aluminum alloy employing a modified butt joint configuration : Influences of process variables

on the weld interfaces and tensile properties, Mater Des 53 (2014) 838–848. https://doi.org/10.1016/j.matdes.2013.07.019.

[23] Z. Ma, Y. Jin, S. Ji, X. Meng, L. Ma, Q. Li, A general strategy for the reliable joining of Al/Ti dissimilar alloys via ultrasonic assisted friction stir welding, J Mater Sci Technol 35 (2019) 94–99. https://doi.org/10.1016/j.jmst.2018.09.022.

[24] S. Zandsalimi, A. Heidarzadeh, T. Saeid, Dissimilar friction-stir welding of 430 stainless steel and 6061 aluminum alloy: Microstructure and mechanical properties of the joints, Proceedings of the Institution of Mechanical Engineers, Part L: Journal of Materials: Design and Applications 233 (2019) 1791–1801. https://doi.org/10.1177/1464420718789447.

[25] P.L. Threadgill, A.J. Leonard, H.R. Shercliff, P.J. Withers, Friction stir welding of aluminium alloys, International Materials Reviews 54 (2009) 49–93. https://doi.org/10.1179/174328009X411136.

[26] S. Shankar, P. Vilaça, P. Dash, S. Chattopadhyaya, S. Hloch, Joint strength evaluation of friction stir welded Al-Cu dissimilar alloys, Measurement 146 (2019) 892–902. https://doi.org/10.1016/j.measurement.2019.07.019.

[27] H. zhong LI, Z. xiao ZHU, X. peng LIANG, P. wei LI, Y. long QI, F. LV, L. HUANG, Effect of T6-treatments on microstructure and mechanical properties of forged Al-4.4Cu-0.7Mg-0.6Si alloy, Transactions of Nonferrous Metals Society of China (English Edition) 27 (2017) 2539–2547. https://doi.org/10.1016/S1003-6326(17)60282-6.